Eur. J. Mech. B/Fluids, **17**, n° 4, 471–488, 1998

Identification and analysis of vortical structures

S. KIDA *, H. MIURA

ABSTRACT. – Various identification and visualization methods of vortical structures, especially of slender vortices, are critically reviewed with a special attention to their objectivity. The sectional-swirl-and-pressure-minimum scheme is presented as a new identification method and applied to homogeneous turbulence. Since the physical quantities associated with an individual vortex can be analyzed separately, this new scheme enables us to investigate quantitatively various physical characteristics related to vortices, such as the variations of the core shape, the circulation and the vorticity vector along a vortex and the temporal evolution of arbitrarily selected vortices. © Elsevier, Paris

1. Introduction

Most flows of practical importance are rotational. Among various kinds of vortical motions, the existence of swirling slender vortices with relatively large vorticity is ubiquitous. Tornadoes in nature, streamwise vortices in turbulent shear flows with or without boundary, Kelvin-Helmholtz vortex rolls and braids in mixing layers and the tubular regions (so-called "worms") of high vorticity in isotropic turbulence are only some of typical examples (Kim *et al.*, 1971; Siggia, 1981; Bernal and Roshko, 1986; Yamamoto and Hosokawa, 1990; Lesieur and Métais, 1996; Kida and Tanaka, 1994). These structures are considered to be generated by various flow instabilities such as the Kelvin-Helmoltz instability and intensified by vortex stretching (Porter *et al.*, 1994; Kida and Tanaka, 1994).

Vortical motions make fluid flows fully three dimensional and complicated in general, and they play a dynamically important role in kinetic energy production and dissipation, mixing, diffusion and transport of mass, heat and momentum, enhancement of frictional drag in turbulent boundary layers, fluid instabilities, and so on. Understanding of the dynamics of vortical structures, such as their generation, interaction and evolution mechanisms, is a prerequisite for flow prediction and control.

Although typical vortices such as those mentioned above are relatively easily recognized, it is surprisingly difficult to define the general vortical structure objectively and unambiguously. Various methods of identification and visualization of slender swirling vortices have been proposed so far by resorting to various flow quantities such as streamlines, pathlines, vorticity, pressure, the Laplacian of pressure, the rate-of-strain tensor, etc. (*see* Lugt, 1979; Jeong and Hussain, 1995). We must admit, however, that there is still no objective criterion with which the vortical structure can be clearly educed and analyzed. Needless to say, it is helpful in the study of fluid dynamics to share a common idea or a consensus on the fundamental processes of fluid motions, e.g. on vortices and waves. In view of the common occurrence of slender vortices, it is highly desirable to arrive at a precise definition.

Theory and Computer Simulation Center, National Institute for Fusion Science, Oroshi 322–6, Toki, Aichi 509–5292, Japan
E-mail: kida@toki.theory.nifs.ac.jp
* Correspondence and reprints

In Section 2, various identification methods of vortical structures are discussed from the point of view of their objectivity. A new vortex eduction scheme is proposed in which the axis and the core of a vortex are determined by tracing the pressure-minimum line under a swirl condition. The advantage of the vortex skeleton representation is emphasized. This scheme is then applied to homogeneous turbulence in Section 3. Section 4 is devoted to a summary and further discussion.

2. Visualization of vortices

We survey here various methods of visualization of vortical structures with special attention given to slender swirling vortices.

2.1. Velocity and vorticity representations

A precise definition of the vortical structure, if any, may be helpful not only for the description of fluid motion but also for discussions of vortex dynamics. The difficulty in arriving at an objective definition, however, has long been recognized among fluid dynamicists (*see* Lugt, 1979). For example, streamlines or pathlines are seen as spiral curves around a vortex by an observer who moves with that vortex. But we do not know *a priori* where the vortex in question is. This leads to a serious problem because the streamline pattern can be different in inertial systems moving with different velocities. Moreover, even if proper streamlines were obtained, it would not be easy to define the vortical domains from their three-dimensional pattern. In the special case when the direction of vortices is known *a priori*, however, streamlines may be useful for identification at least approximately. In fact, the position and the core size of streamwise vortices in wall turbulence were detected by analyzing the streamline pattern projected on cross-stream planes (Bernard *et al.*, 1993). Since, however, streamwise vortices are inclined quite a bit with respect to the streamwise direction both in the wall-normal and spanwise directions (*see* Jeong *et al.*, 1997), this method may suffer from ambiguity.

Vorticity, which is equal to half of the angular velocity of rotation of fluid elements, is one of the most natural candidates for the characterization of vortical motions. A bundle of vorticity lines were used for the visualization of the vortical structure of tubular vortices in isotropic turbulence (She *et al.*, 1991). The hairpin vortices present in wall turbulence were depicted in terms of vorticity lines (Moin and Kim, 1982). In spite of these suggestive studies, we must be careful in representing vortices as vorticity-lines. Vorticity lines are generally chaotic in fully-three-dimensional flows and their topology is structurally unstable. That is, the spatial structure of a vorticity line can change drastically by only slight shifts. Furthermore, the strength of vorticity is not represented by vorticity lines.

Instead of lines, isosurfaces of vorticity magnitude have been used frequently to visualize vorticity concentrations in various turbulent flows partly because of their easy use. In fact, it was by this representation that tubular vortices in isotropic turbulence were first brought to the attention of fluid dynamicists (*see* Siggia, 1981; Yamamoto and Hosokawa, 1988). The formation of tubular vortices from flat vortical structures through the Kelvin-Helmholtz instability was observed in decaying isotropic turbulence (Porter *et al.*, 1994). The use of vorticity magnitude as a representation for swirling tubular vortices, however, is problematic in at least the following two respects. First, solely vorticity cannot distinguish between swirling motions and shearing motions. Recall that Couette flow is rotational but all streamlines are parallel. In fact swirling tubular vortices and shearing flat vortices are characterized by comparing the relative magnitude of vorticity with respect to the rate-of-strain (Tanaka and Kida, 1993). Secondly, the geometrical structure of the isosurfaces varies with threshold, *i.e.* with the value of the vorticity magnitude. Lower thresholds may provide flatter structures. Hence, this representation is subjective if the choice of the threshold remains arbitrary.

A more elaborate characterization of the structure of the velocity field is given by the use of the velocity gradient (or the rate-of-deformation) tensor

$$W_{ij} = \frac{\partial u_i}{\partial x_j}. \tag{1}$$

A classification of the flow topology is made in terms of the three invariants of $\underline{\underline{W}}$ as follows (Dallmann, 1983; Chong *et al.*, 1990).

Consider the topological structure of the velocity field around an arbitrary point in a coordinate system moving with the velocity of the fluid at that point. In the vicinity of this point the velocity field is approximated by

$$u_i = W_{ij} x_j, \tag{2}$$

repeated indices being summed up over 1–3. For an incompressible flow, the eigenvalues λ of $\underline{\underline{W}}$ are calculated from

$$\lambda^3 + Q\lambda + R = 0, \tag{3}$$

where

$$Q = -\frac{1}{2} W_{ij} W_{ji} = -\frac{1}{2} (S_{ij} S_{ji} + \Omega_{ij} \Omega_{ji}) = -\frac{1}{2} (S_{ij} S_{ij} - \frac{1}{2} \omega_k \omega_k) = \frac{1}{2} \nabla^2 p \tag{4}$$

and

$$R = -\frac{1}{3} W_{ij} W_{jk} W_{ki} = \frac{1}{3} (S_{ij} S_{jk} S_{ki} + 3\Omega_{ij} \Omega_{jk} S_{ki}) \tag{5}$$

are the second and third invariants of $\underline{\underline{W}}$ respectively, $S_{ij} = \frac{1}{2}(W_{ij} + W_{ji})$ and $\Omega_{ij} = \frac{1}{2}(W_{ij} - W_{ji}) = -\frac{1}{2} \varepsilon_{ijk} \omega_k$, ($\omega_i$ being the vorticity and ε_{ijk} the Eddington alternating tensor) are the symmetric and anti-symmetric parts of the velocity gradient tensor, respectively. The last equality in (4) is derived by taking the divergence of the Navier-Stokes equations for an incompressible fluid of unit density.

Equation (3) can have either only real roots, or one real root and a conjugate pair of complex roots according to whether the discriminant

$$\Delta \equiv \left(\frac{1}{3} Q\right)^3 + \left(\frac{1}{2} R\right)^2 \tag{6}$$

is non-positive or not. If the eigenvalue is complex at some point, the streamlines around this point form in general spiral curves on a plane spanned by the real and imaginary parts of the eigenvector associated with this complex eigenvalue. The regions in which the eigenvalues of the velocity gradient tensor are complex may be regarded as "vortex" (Dallmann, 1983; Chong *et al.*, 1990). This definition ($\Delta > 0$) of vortical regions will be applied to homogeneous turbulence in the next section. Note that the discriminant is non-positive ($\Delta \leq 0$) for an irrotational flow $\underline{\underline{\Omega}} = \underline{\underline{0}}$ (the equality holds when any two of the eigenvalues are equal). Note also that if $Q > 0$, then $\Delta > 0$.

2.2. Pressure representation

Around the center of a swirling vortex the pressure is likely to be reduced to counterbalance the centrifugal force. This fact suggests a possible use of low-pressure regions for the eduction of vortices. In fact, pressure

has been used by many researchers for the classification of flow structures (Wray and Hunt, 1990) and a better identification of vortical regions in two-dimensional flows (Iwayama and Okamoto, 1996). The superiority of vortex visualization by means of pressure rather than vorticity magnitude has been noticed by Métais and Lesieur (1992) in the case of mixing layer turbulence. Low-pressure regions are easily visualized by bubbles in laboratory experiments. The existence of low-pressure slender vortices in rotating turbulence was reported by Douady *et al.* (1991).

One important thing to be noticed in the pressure representation method is that the minimum of the pressure inside a swirling vortex is relative to the surroundings and that the absolute value of pressure depends on the surrounding pressure distribution. This may bring a serious difficulty in visualizing many vortices at a single pressure level. The visualization of vortices by pressure therefore may not be appropriate for systems in which many vortices coexist, though it can work as a good indicator for the detection of a few strong vortices. Since the choice of the threshold is arbitrary, this method is not objective.

Another fundamental question is that low pressure does not necessarily imply the existence of swirling motion, and vice versa. There is an unsteady flow in which the pressure is lower even if there is no swirling motion. Also pressure does not reach a minimum across a stationary Kármán swirling vortex (Jeong and Hussain, 1995). Our new swirl condition will be discussed in §2.4.

As mentioned above, the pressure level inside of vortices depends on the surrounding flow field and it is not appropriate to visualize many vortices simultaneously. One of the quantities which is free from this drawback but still capable of representing the lower pressure regions is the Laplacian of the pressure $\nabla^2 p$. As shown in (4), this expresses the difference in magnitude between the anti-symmetric and the symmetric parts of the velocity gradient tensor, or the relative magnitude of the vorticity and the strain rate. It was observed in homogeneous shear turbulence that tubular vortices and flat vortical regions appear in the vorticity- and the strain-dominant regions, respectively (Tanaka and Kida, 1993). Since, however, the threshold is set arbitrarily, this method cannot escape from subjectivity.

The above argument regarding the low pressure inside a vortex is applied across the vortex but not along it. That is, the pressure does not necessarily reach a minimum along a vortex. This condition is expressed mathematically by stating that at least two eigenvalues of the pressure Hessian $(\partial^2/\partial x_i \partial x_j)p$ are positive. Considerations aimed at extracting the effects of pressure associated with swirling motion have recently been made by Jeong and Hussain (1995). By removing the effects of unsteadiness and viscosity, which have no direct connection with swirling motions, from the Navier-Stokes equations, they took $-(S_{ik}S_{kj} + \Omega_{ik}\Omega_{kj})$ in place of the pressure Hessian and defined a vortex core as regions in which two eigenvalues of $-(S_{ik}S_{kj} + \Omega_{ik}\Omega_{kj})$ are positive. Note that the set of eigenvalues of $-(S_{ik}S_{kj} + \Omega_{ik}\Omega_{kj})$ does not, in general, coincide with that of the pressure Hessian though the sum of the three eigenvalues does. Therefore the pressure does not always reach a minimum in the regions extracted by this method. This definition (called the λ_2-definition) was applied to several typical flows with clear vortical structures and was shown to be superior to other methods in many respects. This is an objective definition of vortical structures. If this method is applied to homogeneous turbulence, however, the isosurfaces cover too much space to visualize the vortex structure neatly (Miura and Kida, 1997). Note also that contrary to the λ_2-definition, a non-zero threshold for λ_2 is employed in the eduction of the longitudinal vortices in wall-turbulence (Jeong *et al.*, 1997).

2.3. Vortex skeleton

In all the visualization methods of vortical regions discussed in the preceding subsections a finite volume of vortical regions is considered. The size, shape and position of vortical regions not only change in time but also

vary from vortex to vortex. Enormous amounts of memory and computational time are necessary to represent the whole structure and its temporal evolution.

It is now commonly believed, however, that tubular vortices are dominant in most turbulent flows. The core radius, which is several times the Kolmogorov length scale (*see* §3), decreases with Reynolds number. If a vortex is sufficiently thin, we may represent it by its central axis and disregard the core. This is called the vortex skeleton (The core representation will be considered in §2.4).

The skeleton representation has the following merits. First, the amount of data and computation necessary to represent a vortex can be drastically reduced. This makes it possible to describe, for example, the temporal evolution of a vortex. Secondly, each vortex can be marked independently. This permits to visualize only a few arbitrarily chosen vortices. (It is impossible for the isosurface representation of a scalar field to distinguish between individual vortical structures). Then, we can investigate the temporal evolution of selected vortices from their birth to their death, mutual interactions, collisions, breakdown, instabilities, etc. Thirdly, by constructing the core around the axis (e.g. by the use of the swirl condition described in §2.4), we may analyze the temporal evolution of the core deformation. A quantitative analysis of various physical quantities related to vortices is also possible, such as contributions of vortices to the enstrophy and energy-dissipation rate.

The vortex skeleton is constructed for example by tracing the lines of sectional pressure minimum introduced in the preceding subsection. The pressure minimum was searched in planes normal either to the vorticity (Banks and Singer, 1995) or to the third eigenvector, associated with the smallest eigenvalue of the pressure Hessian (Miura and Kida, 1997). The existence of swirling motions around these skeletons has been demonstrated in Figure 2 of Miura and Kida (1997). These two methods are expected to give comparable results for strong slender vortices for which the above two planes are more or less parallel (see *Fig. 5a*). The vortex core is determined by setting an appropriate threshold for the pressure in the former and by the swirl condition (§2.4) in the latter. Note that the latter scheme is objective, but the former is not. Vortices identified by these schemes may conveniently be called low-pressure vortices. An application of the latter scheme to homogeneous turbulence will be presented in §3. Other methods of skeleton construction in which regions of strong vorticity are searched for, have been proposed by Villasenor and Vincent (1992) and by Jiménez *et al.* (1993).

2.4. Swirl condition

As mentioned in §2.2, swirling motion is not always associated with a sectional pressure minimum. In order to educe only swirling vortices we have to impose a swirl condition.

Let us take an arbitrary point in a flow and consider the topological structure of the velocity field in a plane passing through it. Let us choose a Cartesian coordinate system (x_1, x_2, x_3) which moves with the fluid velocity at the above point and whose x_1- and x_2-axes lie in the above plane. In the vicinity of this point, the velocity projected on the (x_1, x_2) plane is written as

$$u_1 = W_{11}x_1 + W_{12}x_2, \tag{7}$$

$$u_2 = W_{21}x_1 + W_{22}x_2 \tag{8}$$

(*see* (2)). The topological structure of the streamlines is characterized by the sign of the discriminant of the (2,2)-matrix $\{W_{ij}\}(i,j = 1,2)$:

$$D = \frac{1}{4}(W_{11} - W_{22})^2 + W_{12}W_{21}. \tag{9}$$

The streamlines are spiral or not around the origin according to whether D is negative or not (If an axisymmetric source or sink flow centered at the origin $u_i = \frac{1}{2}(W_{11} + W_{22})x_i$, $i = 1, 2$ is substracted, the streamlines of the remaining solenoidal flow field form ellipses or hyperbolas according to whether $D < 0$ or $D > 0$.). The elliptical regions may be regarded as vortices (Weiss, 1991; McWilliams, 1984; Brachet *et al.*, 1988). Note that in two-dimensional incompressible flow $W_{11} + W_{22} = 0$ and $D = -Q = -\frac{1}{2}\nabla^2 p$. The definition $Q > 0$ for vortical regions is therefore equivalent to the above definition.

In order to check the rationality of the above definitions of vortical structures we apply them to a Burgers vortex tube, the velocity field of which is written in a cylindrical polar coordinate system (r, θ, z) as

$$u_r = -\frac{1}{2}\alpha r, \tag{10}$$

$$u_\theta = \frac{\Gamma}{2\pi r}\left\{1 - \exp\left[-\frac{\alpha}{4\nu}r^2\right]\right\}, \tag{11}$$

$$u_z = \alpha z, \tag{12}$$

where $\alpha(> 0)$ and Γ are constants.

The vorticity is pointed in the z-direction and is written as

$$\omega_z = \frac{\alpha\Gamma}{4\pi\nu}\exp\left[-\frac{\alpha}{4\nu}r^2\right]. \tag{13}$$

The 1/e (≈ 0.37) radius of the vorticity core is $2\sqrt{\nu/\alpha}$. The pressure is given by

$$\frac{p}{\rho} = -\frac{1}{2}\alpha^2 z^2 - \frac{1}{8}\alpha^2 r^2 - \left(\frac{\Gamma}{2\pi}\right)^2 \int_r^\infty \frac{1}{r_1^3}\left\{1 - \exp\left[-\frac{\alpha}{4\nu}r_1^2\right]\right\}^2 \mathrm{d}r_1 + const. \tag{14}$$

The azimuthal velocity u_θ has a peak at $r_* \approx 2.24\sqrt{\nu/\alpha}$, at which point the vorticity is smaller than that at the center by a factor of 0.18. The circulation and the enstrophy included in a circular cylinder of radius r_* are about 82% of the total. The discriminant D takes negative values at $r < r_*$ so that the present definition of a vortex specifies the core region of a Burgers vortex tube unambiguously. On the contrary, the pressure depends on the strength α of the converging flow. The definition of a vortical structure in terms of pressure, such as $\partial^2 p/\partial r^2$, therefore cannot be universal.

Next we extend the above swirl condition to a plane of arbitrary orientation. In order to do so, we introduce a rotation in which the original Cartesian coordinate system (x_1, x_2, x_3) is rotated around the x_3-axis by an angle $\phi(0 \le \phi \le 2\pi)$ and around a new x_2-axis by an angle $\theta(0 \le \theta \le \pi)$. The velocity field (u_1^*, u_2^*, u_3^*) in the new coordinate system (x_1^*, x_2^*, x_2^*) is then expressed as

$$u_i^* = M_{ia} W_{ab} \widetilde{M}_{bj} x_j^* (\equiv W_{ij}^* x_j^*, \text{say}), \tag{15}$$

where

$$\underline{\boldsymbol{M}} = \begin{pmatrix} \cos\theta\,\cos\phi & \cos\theta\,\sin\phi & -\sin\theta \\ -\sin\theta & \cos\phi & 0 \\ \sin\theta\,\cos\phi & \sin\theta\,\sin\phi & \cos\theta \end{pmatrix} \tag{16}$$

is a rotation matrix and $\underline{\tilde{M}}$ is its inverse. The swirl condition in the (x_1^*, x_2^*) plane is written as

$$
\begin{aligned}
(17) \qquad D(\theta,\phi) &= \frac{1}{4}(W_{11}^* - W_{22}^*)^2 + W_{12}^* W_{21}^* \\
&= \frac{1}{4}[(\cos^2\theta\cos^2\phi - \sin^2\phi)W_{11} + (\cos^2\theta\sin^2\phi - \cos^2\phi)W_{22} + \sin^2\theta W_{33} \\
&\quad + (\cos^2\theta + 1)\sin\phi\cos\phi(W_{12} + W_{21}) - \sin\theta\cos\theta\sin\phi(W_{23} + W_{32}) \\
&\quad - \sin\theta\cos\theta\cos\phi(W_{31} + W_{13})]^2 \\
&\quad + [\cos\theta\cos\phi\sin\phi(W_{22} - W_{11}) + \frac{1}{2}\cos\theta(\cos^2\phi - \sin^2\phi)(W_{12} + W_{21}) \\
&\quad - \frac{1}{2}\sin\theta\cos\phi(W_{23} + W_{32}) + \frac{1}{2}\sin\theta\cos\phi(W_{31} + W_{13})]^2 \\
&\quad - \frac{1}{4}[\cos\theta(W_{12} - W_{21}) + \sin\theta\cos\phi(W_{23} - W_{32}) + \sin\theta\sin\phi(W_{31} - W_{13})]^2.
\end{aligned}
$$

It is obvious that $D(\theta,\phi) \geq 0$ for an irrotational flow in which the anti-symmetric part of the velocity gradient tensor vanishes. Moreover, it is easily shown that there exists a direction (θ,ϕ) for which $D(\theta,\phi) = 0$ in any irrotational flow. This means that at any point in rotational regions (where the vorticity is non zero) there is a plane on which the instantaneous streamlines relative to the velocity at this point are elliptical. In other words, if we define the vortical regions as those at which the minimum (over all orientations) of D is negative, then it covers the whole space. Incidentally, the sectional swirl of streamlines in a plane does not necessarily mean the spiral form of the streamlines viewed from a direction normal to the plane.

The swirl condition $(D(\theta,\phi) < 0)$ is used to supplement the sectional-pressure-minimum scheme for the purpose of picking up swirling vortices. Here, the angles (θ,ϕ) are given by the direction of the third eigeivector of the pressure Hessian [1]. The vortex core is defined as the region $D(\theta,\phi) < 0$ surrounding the vortex axis. This definition (called the sectional-swirl-and-pressure-minimum scheme) of the axis and of the vortex core will be applied to homogeneous turbulence in the next section.

3. Vortical structures in homogeneous turbulence

In this section the low-pressure vortices in freely decaying homogenous turbulence are visualized by making use of the sectional-swirl-and-pressure-minimum scheme described in the preceding section.

3.1. Isotropic turbulence

The vortical structures in isotropic turbulence are analyzed from the data obtained by a direct numerical simulation of the Navier-Stokes equations in a periodic cube of side 2π. The initial velocity field is given in spectral representation with a prescribed energy spectrum $E(k) = (k/k_0)^4 \exp[-2(k/k_0)^2](k_0 = 4)$ with randomized phases. The dealiased (by the shifted-grid technique) spectral method is used for the spatial integro-differential operations with resolution $N^3 = 128^3$. Temporal marching is performed by a fourth-order Runge-Kutta scheme with time step $\Delta t = 5$. Viscosity is set at $\nu = 5 \times 10^{-5}$.

The entrosphy increases at first, takes a maximum and then decreases in time. Here, we consider the flow field at a time after the enstrophy maximum when the smallest scales of motion are fully excited and the

[1] About 20% of the skeleton candidates are discarded by enforcing this condition in homogeneous turbulence as discussed in §3.

tubular vortices are well developed. The Taylor micro-scale λ and the Kolmogorov scale $l_K = \varepsilon^{-\frac{1}{4}} \nu^{\frac{3}{4}}$ at this time are 0.31 and 0.028 respectively, which may be compared with the effective mesh-size of the simulation $\Delta x = 2\pi/128 = 0.049$. The micro-scale Reynolds number R_λ is 46.

In Figures 1, we plot the isosurfaces of (a) the vorticity magnitude and (b) the Laplacian of pressure. The thresholds of these surfaces are chosen in such a way that they cover 5% of the total volume. In both figures, tubular vortical structures are prominent. They look quite similar as a whole, but layered structures are also conspicuous in the vorticity magnitude plots. It should be remembered here that the appearance of the vortical structures displayed through these traditional visualization methods does change substantially depending upon the value of the arbitrarily chosen threshold. That is, they are not objective visualizations.

The central axes of swirling vortices constructed by the sectional-swirl-and-pressure-minimum scheme are drawn with a series of segments of length of order Δx in Figure 2. There are 13302 vortices and their total length is 1660 $(= 33810\Delta x)$. The mean length of the vortices is 0.12 $(= 2.5\Delta x)$, the maximum is 4.1, and the majority (50%) is concentrated in the range between 0.1 and 0.5. Note, however, that since each vortex is easily torn apart by mutual interactions, it is not so meaningful to speak about their mean length. As discussed in Miura and Kida (1997), all the skeletons of low-pressure vortices are not included in the isosurfaces of the vorticity magnitude nor of the pressure Laplacian.

In order to see the characteristic features of the vortices in more detail we plot in Figure 3a the variations of D (solid line), $\frac{1}{2}|\boldsymbol{\omega}|^2$ (thick broken line), p (dotted line) and $\nabla^2 p$ (thin broken line) along the axis of an arbitrarily chosen vortex (the light-blue one in Figure 7). The abscissa is the arc-length s (measured from the right-end of the above vortex in Figure 7) scaled by the mesh-size Δx. The axial length of this vortex is $50\Delta x$. It is remarkable that there is a strong correlation between the variations of the three physical quantities, namely, $\frac{1}{2}|\boldsymbol{\omega}|^2$, $\nabla^2 p$ and $-D$ change in the same sense, and also a weak correlation with $-p$. A similar behavior is observed in other vortices as well. This accounts for the fact that either high $|\boldsymbol{\omega}|^2$, high $\nabla^2 p$, low p or low D has often been used for the visualization of vortices.

The cross-sections of the core (defined as regions where $D < 0$) are depicted over the whole vortex in Figure 3b. The ordinate is normalized by the Kolmogorov length scale. It is seen that the shape of the cross-section varies substantially from place to place, as commonly observed in other vortices as well. The variation of the cross-section in the range $25 < s/\Delta x < 35$ (around the lowest D) is enlarged in Figure 3c. The shape is roundish and stable in this range.

The radius from the center to the core periphery varies in general with the direction (see *Figs.* 3b and c). The mean (thick line) and the standard deviation (broken line) along the vortex axis are shown in Figure 4a. The mean value is more or less stable especially where the core is round (see *Fig.* 3c).

It is not easy to estimate the mean core radius of vortices because both the shape and the area change a lot from vortex to vortex. But since the core of long vortices is relatively round, we may define reasonably well the mean radius of relatively long vortices. The mean radius averaged over all vortices is $3.2l_K$, while it is $3.8l_K$ for vortices whose length is larger than the mean. The mean value increases with the threshold of the length and approaches around $4.5l_K$. Here, the average has been taken over relatively round cores whose radius does not exceed $\pm$ 30% of the mean in all directions. Comparable values were obtained before by Jiménez *et al.* (1993) and Tanahashi *et al.* (1997). In the latter the azimuthal velocity is shown to be well approximated by that of the Burgers vortex (11).

The distribution of the circulation Γ along the vortex axis is shown in Figure 4b. Here, the circulation is calculated by direct numerical integration of the velocity around the core periphery. It varies gradually except for a rather rapid change around $s/\Delta x = 20$. It takes values of about 0.011 and 0.005 on the right and left sides of the region of rapid change, respectively. The vortex Reynolds number $\mathrm{R}_\Gamma = \Gamma/\nu$ is 220 and 100 respectively

(a)

(b)

Fig. 1. – Isosurfaces of (a) the vorticity magnitude and (b) the Laplacian of pressure in isotropic turbulence. The thresholds are set so that each of them covers 5% of the total volume.

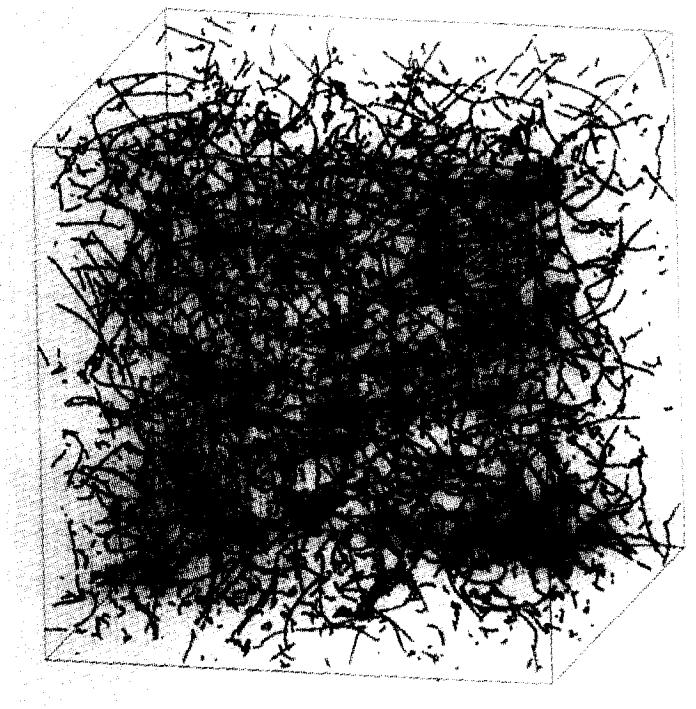

Fig. 2. – Vortex skeletons in isotropic turbulence.

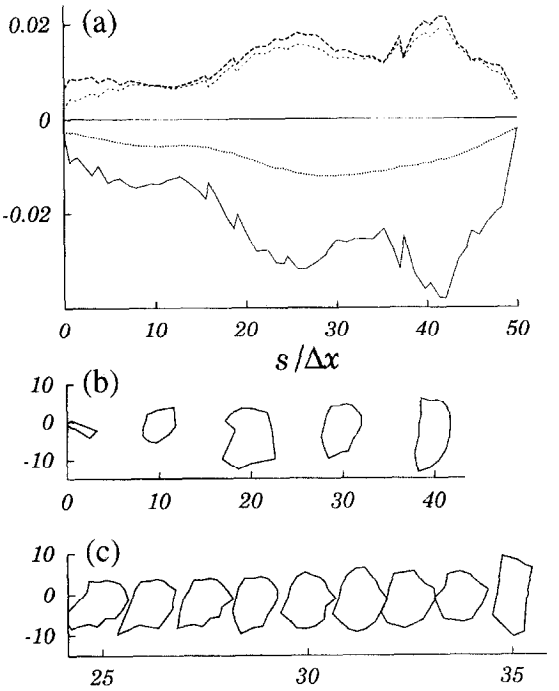

Fig. 3. – (a) Variations of D (solid line), $\frac{1}{2}|\omega|^2$ (thick broken line), p (dotted line) and $\nabla^2 p$ (thin broken line) along the axis of a vortex. Here, p is multiplied by 100. Cross-section of the core (b) in the entire vortex and (c) in range $25 < s/\Delta x < 35$.

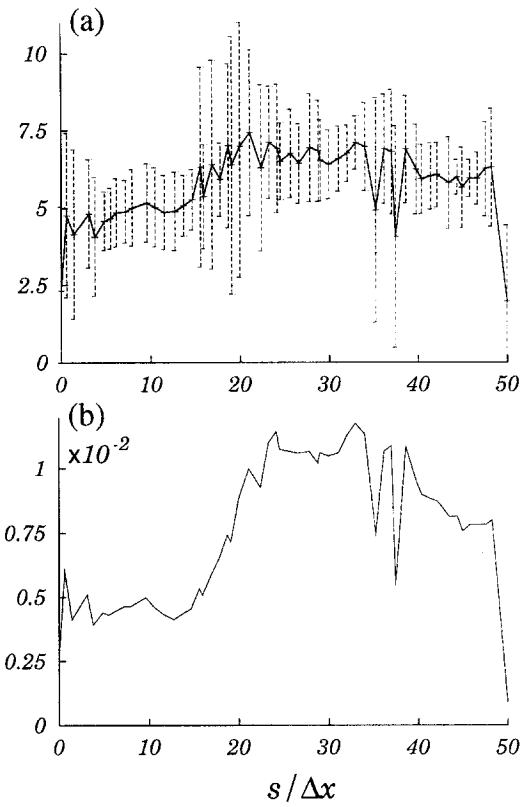

Fig. 4. – Axial distributions of (a) the mean (solid line) and the standard deviation (broken line) of the core radius and (b) the circulation of a vortex.

in each of these ranges. These values may be compared with $R_\Gamma \approx 126$ at $R_\lambda \approx 36$ and $R_\Gamma \approx 135$ at $R_\lambda \approx 63$ which are reported by Jiménez *et al.* (1993). The reduction of the circulation on the left may be attributed to a tear-off of the vortex core by a nearest vortex tube (see *Fig.* 6b below).

The variations of the directions of the third eigenvector of the pressure Hessian (solid line) and the vorticity (broken line) along the above vortex are shown in Figure 5a, in which the angles of these vectors measured from the skeleton direction are plotted. The angles between the two vectors as well as between consecutive segments are shown in Figures 5b and c, respectively. It is seen that both of the angles shown in Figure 5a are relatively small (about 10° or less) over the whole range except at the very right end. This suggests that the two skeleton construction schemes based on either vorticity or pressure Hessian (*see* §2.3) give comparable results though the latter seems slightly better. This angle in the latter should tend to zero in the limit of infinite resolution ($\Delta x \to 0$). The large values at the end indicate that the vortex is kinked strongly there (see *Fig.* 5c).

The vortical regions surrounding the vortex skeletons are educed by the sectional-swirl-and-pressure-minimum scheme described at the end of the preceding subsection. They occupy 41% of the total volume which is so large that the core structure can hardly be seen by plotting the core boundary (figures omitted). The enstrophy included in these vortical regions is 61% of the total. Incidentally, the vortical regions defined by $\Delta > 0$ and $\nabla^2 p > 0$ occupy 65% and 43% of the total volume, respectively. These are again too much for the isosurfaces to visualize the structure well. In our method, however, the visualization of vortices is possible because any vortex skeleton can be chosen and marked arbitrarilly. In Figure 6a, we select 13 vortices whose core regions are drawn with colored surfaces. The vortex presented in Figures 3-5 is the light-blue one. Figure 6b is a close-up of this vortex. It is clearly seen that the core is gouged out by a nearest vortex (green).

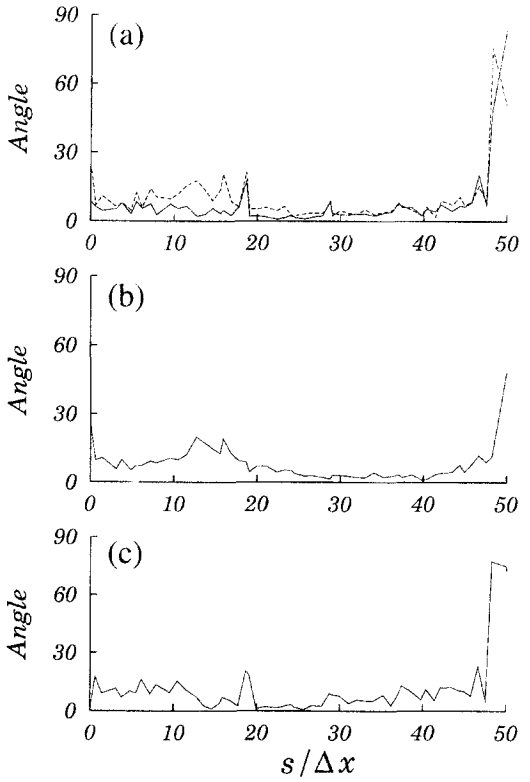

Fig. 5. – Variations along a vortex of (a) the angles of the third eigenvector of the pressure Hessian (solid line) and of the vorticity (broken line) with respect to the skeleton, (b) the angles between the eigenvector of the pressure Hessian and the vorticity, and (c) the angles of consecutive segments of the skeleton.

3.2. Homogeneous shear turbulence

The data for homogeneous shear turbulence which are analyzed here were simulated by Kida and Tanaka (1992, 1994). The simulation was started with a random velocity field superimposed on a uniform mean shear flow $\overline{u}_1 = Sx_2$, where $S(= 10)$ is the shear rate. The subscripts 1, 2 and 3 denote the streamwise, vertical and spanwise directions, respectively. The fluctuating field is periodic with periods 4π, 2π and 2π in the x_1-, x_2- and x_3-directions, respectively. Spatial integro-differential operations were made by a spectral method with resolution $N^3 = 128^3$. Then the effective mesh-size are $\Delta x_1 = 0.098$ and $\Delta x_2 = \Delta x_3 = 0.049$. A Runge-Kutta-Gill scheme with time step $\Delta t = 0.002$ was employed for temporal marching.

In Figures 7, we plot the isosurfaces of (a) the vorticity magnitude and (b) the Laplacian of pressure and (c) their union at $St = 8$ by which time turbulence is well developed. Here, a quarter of the fundamental periodic box ($0 \leq x_1 \leq 4\pi, 0 \leq x_2, x_3 \leq \pi$) is displayed. The levels of the isosurfaces are chosen in such a way that they include 5% of the total volume. The oblique vortical structure inclined vertically with respect to the streamwise direction is common in both fields. However, the shape of the structure is very different in each representation. It is flat in the vorticity magnitude and tubular in the Laplacian of pressure. Most tubular structures in the vorticity magnitude plot are included in the isosurfaces of $\nabla^2 p$, while the flat structures are outside (*see* Tanaka and Kida, 1993). Incidentally, the root-mean-square of the vorticity magnitude is $\sqrt{\langle|\boldsymbol{\omega}|^2\rangle} = 11$ which is comparable with the mean shear vorticity $S = 10$, and the three components of vorticity are of comparable magnitude, $\sqrt{\langle\omega_1^2\rangle} = 11$, $\sqrt{\langle\omega_2^2\rangle} = 10$ and $\sqrt{\langle\omega_3^2\rangle} = 15$.

(a)

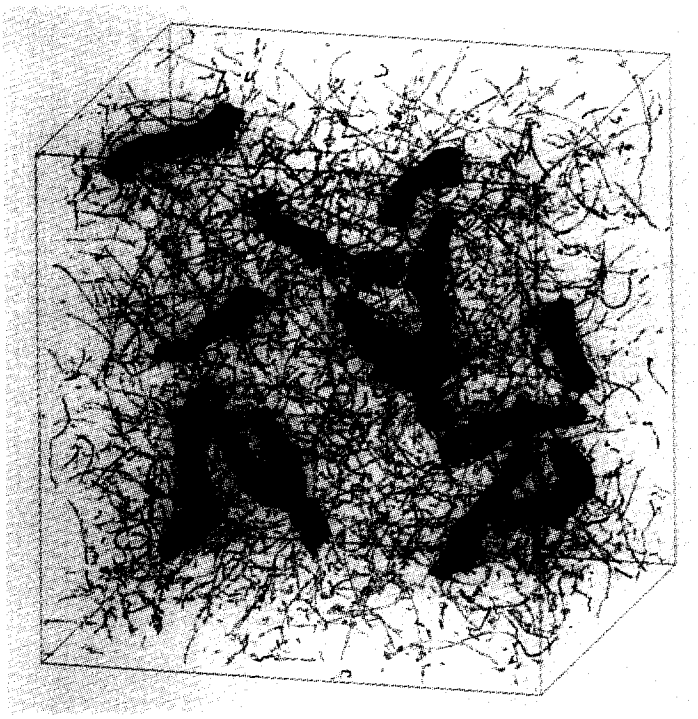

(b)

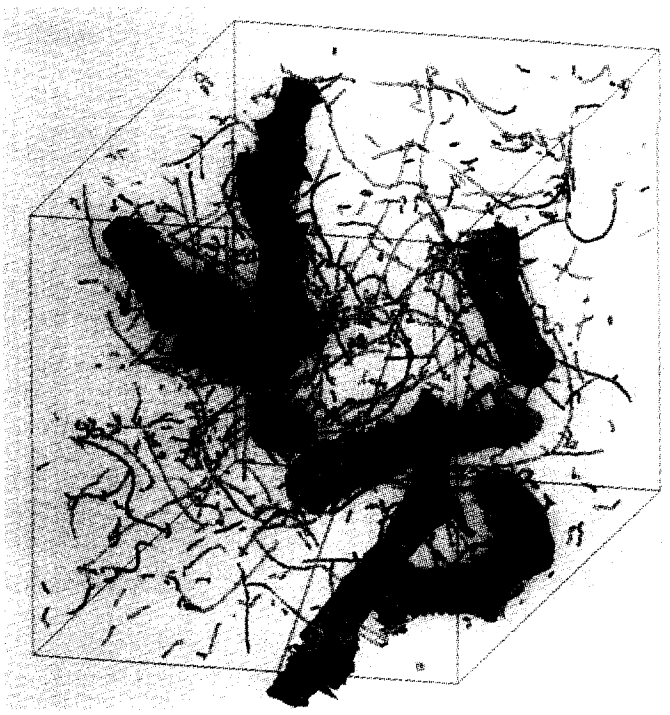

Fig. 6. – Vortex skeletons (white lines) and 13 vortex cores (colored) in isotropic turbulence. (b) Close-up of (a). Part of the core of the light-blue vortex is being gouged out by another vortex (green).

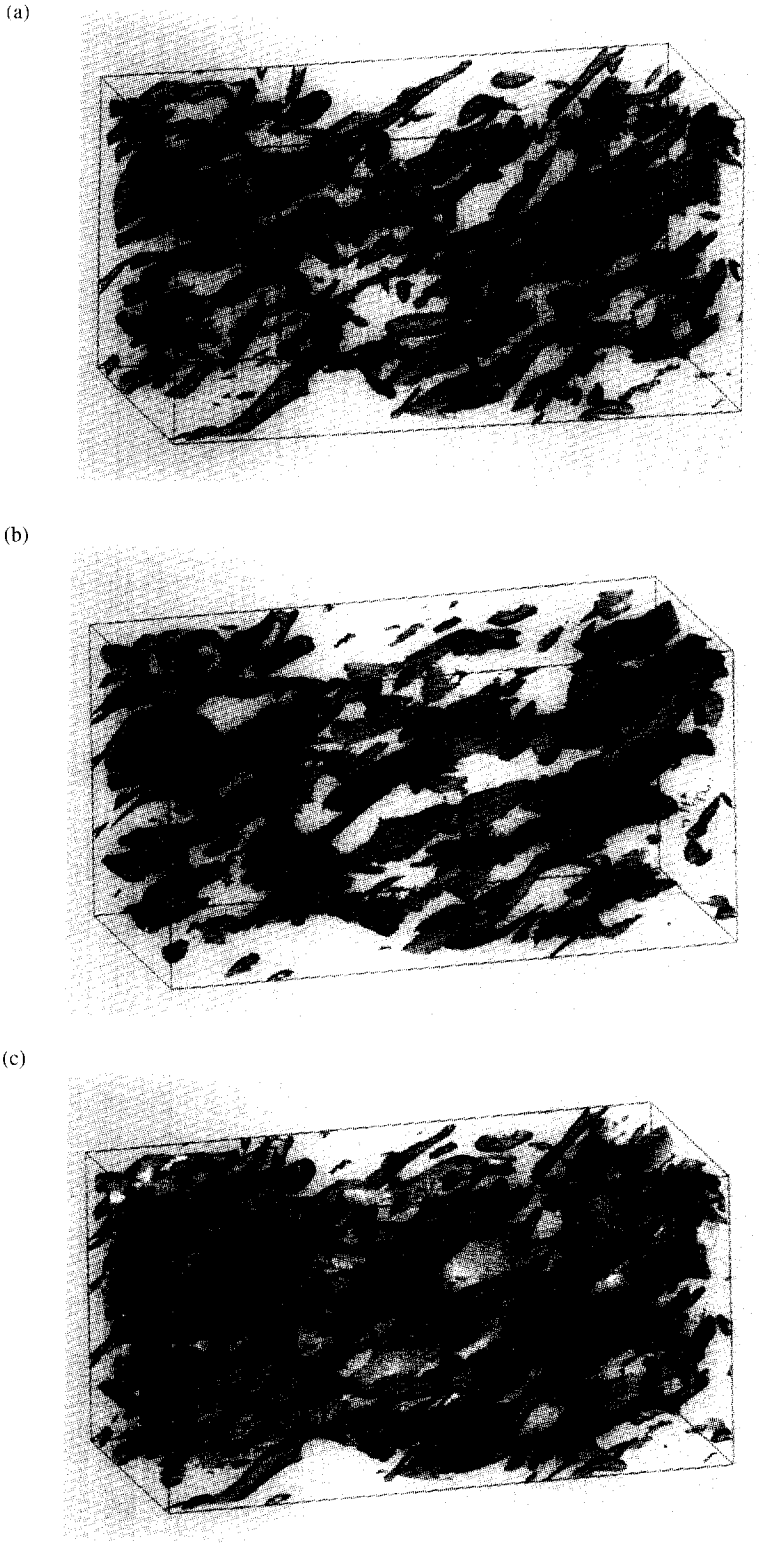

Fig. 7. – Isosurfaces of (a) the vorticity magnitude and (b) the Laplacian of pressure and (c) their union in homogeneous shear turbulence. The thresholds are set so that each of them covers 5% of the total volume.

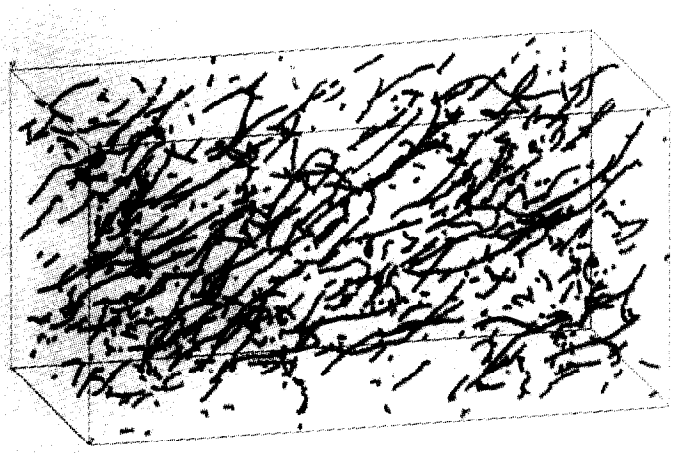

Fig. 8. – Vortex skeletons in homogeneous shear turbulence.

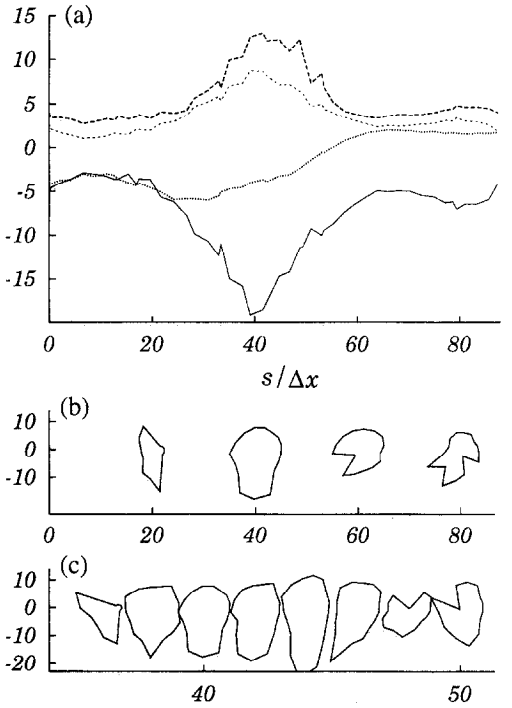

Fig. 9. – (a) Variations of D (solid line), $\frac{1}{2}|\omega|^2$ (thick broken line), p (dotted line) and $\nabla^2 p$ (thin broken line) along the axis of a vortex. Here, p is multiplied by 100. The cross-section of the core (b) in the entire vortex and (c) in the range $35 < s/\Delta x < 50$.

The vortex skeletons constructed by the sectional-swirl-and-pressure-minimum scheme are drawn in Figure 8. There are 2775 vortices and the total length is $311\,(= 6328\Delta x_2)$. The mean length of the vortices is then $0.11(= 2.3\Delta x_2)$. The Kolmogorov length at this time is $l_K = 0.023$. All the skeletons are again not included in the isosurfaces of vorticity magnitude nor the Laplacian of pressure (figures omitted).

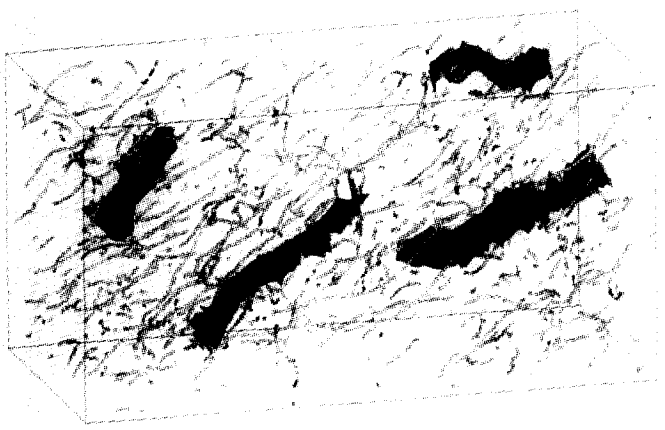

Fig. 10. – Vortex skeletons (white lines) and 4 vortex cores (colored) in homogeneous shear turbulence.

The variations of D, $\frac{1}{2}|\omega|^2$, p and $\nabla^2 p$ along the axis of a vortex (the lower-right one in Figure 10) are plotted in Figure 9a. The meaning of the lines is the same as in Figures 3a. The arc-length is measured from the right end of the above vortex in Figure 10. The axial length of this vortex is $87\Delta x_2$. There is again a strong correlation in the variations of $\frac{1}{2}|\omega|^2$, $\nabla^2 p$ and $-D$ (cf. *Fig.* 3a).

The core cross-section of this vortex is shown in Figures 9b and c over the entire vortex and over $35 < s/\Delta x < 50$ (around the lowest D), respectively. The change of shape is substantial. The mean radius averaged over all vortices is $4.9 l_K$, and it is $5.8 l_K$ for vortices longer than the mean length. The mean value for longer vortices seems to approach around $6.1 l_K$. These values are greater by about 50% than those for isotropic turbulence (§3.1).

The vortical regions defined by $D < 0$ occupy 14% of the total volume which is again too much to visualize their entire boundary. 16% of the enstrophy is included in these vortical regions. The vortical regions defined by $\Delta > 0$ and $\nabla^2 p > 0$ occupy 70% and 44% volume, respectively.

Four vortices have been selected and shown in Figure 10, where the color denotes the sum of the two largest eigenvalues of the pressure Hessian. The green is the largest and the yellow is the lowest. The structure of individual vortices is now clearly visualized.

4. Concluding remarks

We have considered in this paper how to educe and visualize the swirling slender vortices from complicated turbulent motions. The sectional-swirl-and-pressure-minimum scheme has been proposed as one of the objective eduction methods of low-pressure vortices. This scheme is composed of two steps; the trace of the vortex axes and the construction of the core. It is a serious common problem that the required amounts of memory and computation are too enormous to analyze the spatial structure and temporal evolution of three-dimensional vortical structures. Fortunately, we can relax this problem by the use of the above scheme in the following two ways. First, by representing a vortex only by its central axes (the skeleton representation), we can decrease the data size drastically. Secondly, since individual vortices can be marked and analyzed independently, it is possible to pick up only a few vortices to be investigated.

Finally, we would like to mention the case of coherent structures, among which may be counted the swirling slender vortex. Although coherent or organized structures which keep their identity in turbulent flows over

relatively long times and over a wide spatial extent have attracted the attention of researchers for three decades, there does not seem to be a unique method to find and define long-lived structures in continuous fluid flows. Many different kinds of coherent structures can be observed in principle depending upon which physical quantity one focusses on (Hussain, 1986; Robinson, 1991). Our understanding of turbulence may be influenced by the definition adopted for coherent structures. Therefore, it is quite important to find and study such coherent structures that play dynamically essential roles.

Acknowledgements. – The authors would like to thank Professor N. J. Zabusky for introducing us to some relevant references on vortex visualization. Thanks also are due to Dr. M. Tanaka for his kind offer of numerical data for homogeneous shear turbulence. This work was partially supported by a Grant-in-Aid for Scientific Research from the Ministry of Education, Science and Culture in Japan.

REFERENCES

BANKS D. C., SINGER B. A., 1995, A predictor-corrector technique for visualizing unsteady flow, *IEEE Trans. on visualization and computer graphics*, **1**, 151-163.

BERNAL L. P., ROSHKO A., 1986, Streamwise vortex structure in plane mixing layers, *J. Fluid. Mech.*, **170**, 499-525.

BERNARD P. S., THOMAS J. M., HANDLER R. A., 1993, Vortex dynamics and the productions of Reynolds stress, *J. Fluid. Mech.*, **253**, 385-419.

BRACHET M. E., MENEGUZZI M., POLITANO H., SULEM P. L., 1988, The dynamics of freely decaying two-dimensional turbulence, *J. Fluid Mech.*, **194**, 333-349.

CHONG M. S., PERRY A. E., CANTWELL B. J., 1990, A general classification of three-dimensional flow fields, *Phys. Fluids A*, **2**, 765-777.

DALLMANN U., 1983, Topological structures of three-dimensional flow separations, *DFVLR*, Rep. No. 221-82-A07, Göttingen, West Germany.

DOUADY S., COUDER Y., BRACHET M. E., 1991, Direct observation of the intermittency of intense vorticity filaments in turbulence, *Phys. Rev. Lett.*, **67**, 983-986.

HUSSAIN F., 1986, Coherent structures and turbulence, *J. Fluid Mech.*, **73**, 303-356.

IWAYAMA T., OKAMOTO H., 1996, Reconsideration of a scaling theory in two-dimensional decaying turbulence, *Prog. Theor. Phys.*, **96**, 1061-71.

JEONG J., HUSSAIN F., 1995, On the identification of a vortex. *J. Fluid Mech.*, **285**, 69-94.

JEONG J., HUSSAIN F., SCHOPPA W., KIM J., 1997, Coherent structures near the wall in a turbulent channel flow, *J. Fluid Mech.*, **332**, 185-214.

JIMÉNEZ J., WRAY A. A., SAFFMAN P. G. ROGALLO R. S., 1993, The structure of intense vorticity in isotropic turbulence, *J. Fluid Mech.*, **255**, 65-90.

KIDA S., TANAKA M., 1992, Reynolds stress and vortical structure in a uniformly sheared turbulence, *J. Phys. Soc. Japan*, **61**, 4400-4417.

KIDA S., TANAKA M., 1994, Dynamics of vortical structures in a homogeneous shear flow, *J. Fluid Mech.*, **274**, 43-68.

KIM H. T., KLINE S. J., REYNOLDS W. C., 1971, The production of turbulence near a smoth wall in a turbulent boundary layer, *J. Fluid Mech.*, **50**, 133-160.

LESIEUR M., MÉTAIS O., 1996, New trends in large-eddy simulations of turbulence, *Annu. Rev. Fluid Mech.*, **28**, 45-82.

LUGT H. J., 1979, The dilemma of defining a vortex, *Recent Developments in Theoretical and Experimental Fluid Mechanics, Springer*, pages 309-321.

MCWILLIAMS J. C., 1984, The emergence of isolated coherent vortices in turbulent flow, *J. Fluid Mech.*, **146**, 21-43.

MIURA H., KIDA S., 1997, Identification of tubular vortices in complex flows, *J. Phys. Soc. Japan*, **66**, 1331-1334.

MOIN P., KIM J., 1982, Numerical investigation of turbulent channel flow, *J. Fluid Mech.*, **118**, 341-377.

PORTER D. H., POUQUET A., WOODWARD P. R., 1994, Kolmogorov-like spectra in decaying three-dimensional supersonic flows, *Phys. Fluids*, **6**, 2133-2142.

ROBINSON S. K., 1991, Coherent motions in the turbulent boundary layer, *Ann. Rev. Fluid Mech.*, **23**, 601-39.

SHE Z. S., JACKSON E., ORSZAG S. A., 1991, Structures and dynamics of homogeneous turbulence: models and simulations, *Proc. R. Soc. Lond. A*, **434**, 101-124.

SIGGIA E. D., 1981, Numerical study of small scale intermittency in three dimensional turbulence, *J. Fluid Mech.*, **107**, 375-406.

TANAHASHI M., MIYAUCHI T., IKEDA J., 1997, Scaling law of coherent fine scale structure in homogeneous isotropic turbulence, *11th. Symp. on Turbulent Shear Flows* (to be published).

TANAKA M., KIDA S., 1993, Characterization of vortex tubes and sheets, *Phys. Fluids A*, **5**, 2079-2082.

VILLASENOR J., VINCENT A., 1992, An algorithm for space recognition and time tracking of vorticity tubes in turbulence, *COMP: Image Understanding*, **55**, 27-35.

WEISS J., 1991, The dynamics of enstrophy transfer in two-dimensional hydrodynamics, *Physica D*, **48**, 273-294.

WRAY A. A., HUNT J. C. R., 1990, Algorithms for classification of turbulent structures, *In Topological Fluid Mechanics* (ed. H. K. Moffatt & A. Tsinober), pp. 95-104, Cambridge University Press.

YAMAMOTO K., HOSOKAWA I., 1988, A decaying isotropic turbulence pursued by the spectral method, *J. Phys. Soc. Japan*, **57**, 1532-1535.

(Received 26 June 1997,
revised 14 November 1997,
accepted 9 December 1997)